www.sciencemag.org/cgi/content/full/science.aah3398/DC1

Supplementary Materials for

High-quality graphene via microwave reduction of solution-exfoliated graphene oxide

Damien Voiry, Jieun Yang, Jacob Kupferberg, Raymond Fullon, Calvin Lee, Hu Young Jeong, Hyeon Suk Shin, Manish Chhowalla*

*Corresponding author. Email: manish1@rci.rutgers.edu

Published 1 September 2016 on *Science* First Release
DOI: 10.1126/science.aah3398

This PDF file includes:

Materials and Methods

Chemicals and Reagents

Sulfuric acid, potassium permanganate, sodium nitrate, sulfuric acid, nickel nitrate and iron nitrate were purchased from Sigma Aldrich and used as received. SiO_2/Si wafers (300 nm thick SiO_2 layer on a highly doped p-type Si(100)) were purchased from Nova Electronic Materials. Ultra-high purity Argon was purchased from Airgas.

Physical characterization.

Graphene oxide (GO), reduced graphene oxide (rGO), microwaved reduced graphene oxide (MW-rGO) sheet were characterized by a field-emission scanning electron microscope (SEM) with an accelerating voltage of 5 kV. High-resolution transmission electron microscopy (HRTEM) were acquired by a FEI Titan G2 60-300 with an image-forming Cs corrector at an accelerating voltage of 80 kV. MW-rGO and rGO were sonicated in N-methyl-2-pyrrolidone (NMP) and then dropped onto holey carbon TEM grids for analysis. XPS measurements were performed with a Thermo Scientific K-Alpha spectrometer. All spectra were acquired using a microfocused monochromatized source (1,486.7 eV) with a spot size of 400 μm and a resolution of 0.6 eV. All samples for XPS were deposited onto Au substrate. Raman spectra were obtained using a Renishaw 1000 system operating at 514 nm (2.41 eV). CVD-grown graphene was synthesized following methods from the literature (*46*). Data from dispersed graphene were taken from the article by Paton *et al.* (*3*). Reduced graphene oxide is prepared by annealing graphene oxide under argon for 1h at 500°C.

Device fabrication.

Field-effect transistors made of rGO and MW-rGO were fabricated in two-terminal configuration using silver as contacts for both the source and the drain electrodes. Ionic liquid (Bimm PF6) was used as gate dielectric and offers a high double-layer capacitance (C_{dl}) of ~ 20 μF/cm^2. Platinum wire was used as top-gate electrode. Contacts were passivated prior any measurements so that only MW-rGO (rGO) is exposed to the ionic liquid.

Electrochemical Measurements.

The electrochemical measurements were performed in a 3-electrode configuration using a saturated calomel electrode (SCE) and a graphite rod as reference and counter electrodes respectively. The saturated calomel electrode (SCE) was calibrated against platinum under 1 bar of H_2 in a 0.1 M KOH solution saturated with H_2. In 0.1 M KOH, we measured: $E_{RHE} = E_{SCE} + 949$ mV. The electrochemical measurements were carried out using a Multistat 1480 potentiostat from Solartron Group. Electrochemical impedance spectroscopy (EIS) was investigated out using a SI-1260 Impedance/Gain Phase analyzer (Solartron) at $\eta = 0.2$-0.250 V from 10^6 to 0.1 Hz with an alternating current voltage of 10 mV. OER ($2OH^- = ½O_2+H_2O+2e^-$) performance of the electrodes was evaluated in a 0.1 M KOH electrolyte solution. Electrodes were first cycled for > 50 cycles before any measurement in order to stabilize the electrochemical response. Polarization curves were

obtained by sweeping the potential of the working electrode from 0 mV to +900 mV vs. the reference electrode at a scan rate of 5 $mV.s^{-1}$**.**

Graphene oxide (GO) synthesis

GO was prepared from natural graphite by the modified Hummers' method (*19*). Graphite powder (1.5 g) was immerged into cold concentrated H_2SO_4 (50.7 mL) with sodium nitrate (1.14g). $KMnO_4$ (6g) was added slowly while stirring for 2 h. After 3 days, 5% H_2SO_4 solution (150mL) was slowly added and the reaction was finally terminated by the addition of 30% H_2O_2 (4.5 mL), after which the color of the solution changed to bright yellow. The mixture was washed with 10% HCl in order to remove metal ions. The solution was then cleaned via dialysis (molecular weight cut-off = 14,000, Sigma-Aldrich) to remove metal ions and acids completely. The GO product was centrifuged at low speed in order to remove smaller flakes and finally at 6000 rpm for 30 min to concentrate the solution.

Preparation of Microwave reduced graphene oxide (MW-rGO)

The GO solution (5.7 mg/mL) was injected at a 0.1 mL/min of flow rate into a coagulation bath (1 wt%. aqueous $CaCl_2$ solution) using a syringe pump. Coagulated GO was then washed with DI water and dried in air. Mild reduction of GO was carried out by annealing at 300 °C for 1 h under Argon. Mildly reduced GO was placed in a vial and microwaved (Panasonic microwave oven, 1000 W) for 1-2 s under Argon. Upon microwave irradiation, large arcing was observed around GO (Fig. 1). We observed that arcs typically last 50-100 ms, which suggests an extremely fast annealing process during which GO is heated up to several thousands of Celsius in only few tens of ms. Microwaved reduced graphene oxide (MW-rGO) was then allowed to cool for few minutes. No arcs were observed when microwaving GO confirming that mild annealing of GO is crucial.

Fig. S1.
Digital pictures showing the formation of arcs during GO microwaving. Pictures were taken every ~ 50 ms.

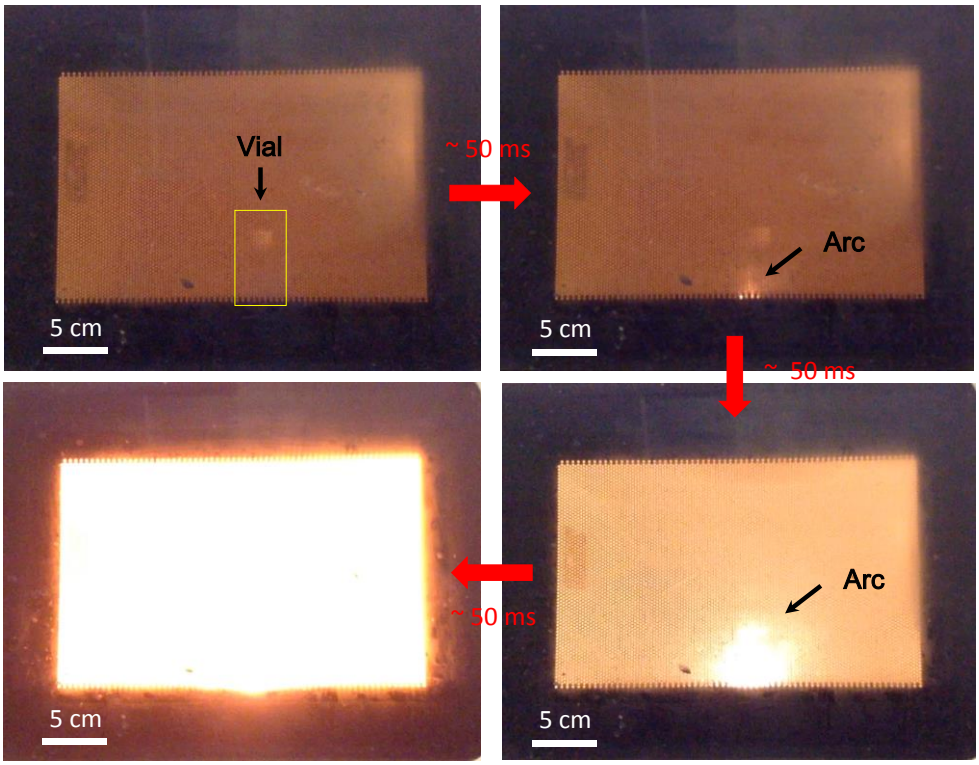

Supplementary Text

Raman spectroscopy of graphene oxide and microwaved reduced graphene oxide

Raman spectroscopy was used in order to estimate the reduction of the different GO-derived samples. Samples were deposited on SiO_2/Si wafer and Raman spectra were corrected to the position of silicon peak at 520 cm^{-1}. Raman spectroscopy is a powerful tool to investigate the structure and thus the intrinsic quality of nanocarbons such as carbon nanotubes and graphene (*47*). Raman spectrum of ideal graphene consists in three main peaks: a D peak at ~ 1350 cm^{-1} coming for the sp^3 carbons from defects (D band is thus virtually absent in high quality graphene), a G peak at ~ 1580 cm^{-1} attributed to the sp^2 carbons and an intense 2D (also noted G') peak at ~ 2700 cm^{-1} that is the second order mode of the D band (*47*, *48*). In monolayer graphene is 2D band is expected to be higher than the G peak (typically 2-3 times higher) and perfectly symmetrical. The influence of defects on the vibrational response of graphene and graphite has been intensively investigated in the last decades (*48–50*). Empirical formula has been deduced from the evolution of the D and G peaks with the distance between defects: L_D (Equation *(Eq. I)*) (49):

$$L_D{}^2(nm^2) = (1.8 \pm 0.5) \times 10^{-9} \times \lambda^4 \times \left(\frac{I_D}{I_G}\right)^{-1}$$ *(Eq. I),*

Where λ (in nm), I_D and I_G represent the wavelength of the Raman laser and the intensity of the D and G band respectively. For L_D > 10 nm, the density of defects, n_D, can be estimated using Equation *(II)* (*50*):

$$n_D(cm^{-2}) = \frac{(1.8 \pm 0.5) \times 10^{22}}{\lambda^4} \times \left(\frac{I_D}{I_G}\right)$$ *(Eq. II)*

The size of the crystalline domains, L_a, can be estimated from the Raman signals using Equation *(Eq. III) (51)*:

$$L_a\ (nm) = (2.4 \times 10^{-10}) \times \lambda^4 \times (\frac{I_D}{I_G})^{-1}$$ *(Eq. III)*

We performed Raman spectroscopy on CVD-grown graphene, graphene oxide and reduced graphene oxide samples deposited on silicon dioxide wafer. High reduction of the graphene oxide after microwaving is clearly seen in Fig. 1D. Notably the D peak intensity is dramatically reduced whereas the restoration of the 2D band clearly shows that the structure of sp^2 carbon for MW-rGO is largely restored. Raman analysis of hundreds of MW-rGO samples reveals that the I_{2D}/I_G ratio is close or higher than 1 whereas the I_G/I_D ratio is larger than 10. Such evolution of the D and 2D peaks largely differs from rGO samples even after annealing at temperatures as high as 1000°C (*23*) or chemical reduction using hydrazine (*52*), hydroiodic acid (*25*), or ascorbic acid (*53*). Table S1 summarizes the main properties of MW-rGO compared to CVD-grown graphene and dispersed graphene (*3*). We also compared the effect of microwaving time on the reduction of the graphene oxide nanosheets and we observed that microwaving pulses as short as 1 - to 2 s - at 1000 W lead to optimal reduction whereas longer time or higher power don't improve further the reduction of graphene oxide. From the Raman spectra it is clear that microwave treatments remove almost completely the oxygen functional groups, restore the crystallinity of the nanosheets and significantly increase the size of sp^2 domains.

Table S1.
Crystal size (L_a), distance between defects (L_D) and defect density (n_D) of MW-rGO compared to CVD-grown graphene and dispersed graphene.

	L_a (nm)	L_D (nm)	n_D (cm^{-2})
CVD-grown graphene	186	36	2.28×10^{10}
Dispersed graphene	90.9	26	4.68×10^{10}
MW-rGO	180 ± 77	38 ± 8	$2.87(\pm 1.45) \times 10^{10}$

It is worth noting that the high I_{2D}/I_G ratio combined to the shape of the 2D peak perfectly symmetrical suggests the presence of single layer nanosheets (Fig. S2). The full width at half maximum (FWHM) of 36 cm^{-1} is close to the value expected for single-layer graphene and much smaller than in the case of randomly stacked single-layer graphene (~ 50 cm^{-1}) (*48*).

Fig. S2.
2D band of MW-rGO together with its lorentzian fit. 2D band is perfectly symmetrical with a FWHM of 36 cm^{-1} suggesting the presence of single-layer MW-rGO.

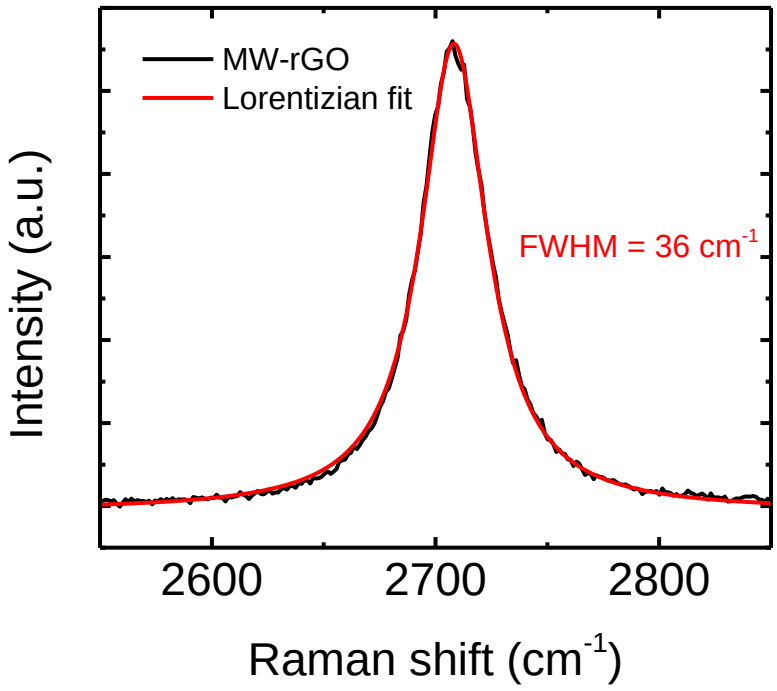

X-ray photoelectron spectroscopy (XPS)

XPS was employed to characterize the surface chemistry of CVD grown graphene, MW-rGO, rGO and GO. The surface chemistry of graphene oxide has been intensively studied in the literature and is composed of various functional groups including epoxy, hydroxyl, ketone, phenol, lactone and carboxylic acid functions. The deconvolution of the C1s spectrum of GO confirms the presence of all these chemical groups on the surface of the graphene oxide nanosheets with peaks at ~ 286.4 eV, ~ 287.8 eV and ~ 288.9 eV attributed to the C-O, C=O and O-C=O bonds respectively in perfect agreement with previous works from the literature (Fig. 1B) (*32*, *54*). Additionally C-C peak from the sp^2 carbons is slightly shifted relative to the peak from the sp^3 hybridized carbons at 284.5 eV and 285 eV respectively and thus the C-C peak can be deconvoluted with 2 lorentzian curves. Upon mild reduction at 500°C, significant amount of oxygen groups are removed as shown in Fig. 1B. At the opposite CVD-grown graphene, which consists in conjugated sp^2 carbons, contains almost no oxygenated chemical groups. Signals for MW-rGO are virtually identical to one obtained for graphene indicating similar surface chemistry (Fig. 1B). Deconvolution of the C1s regions enables to quantify the density of the functional groups as well as the amount of sp^2 and sp^3 carbon atoms. Fig. S3 shows the evolution of the sp^2 atoms with the carbon content for graphene and all the GO-derived samples. It appears clearly that the carbon content in MW-rGO is significantly larger than for mildly reduced rGO: > 90% vs. ~ 70% respectively whereas the percentage of sp^2 carbon atoms is 3 times higher than rGO and very close to CVD graphene.

Fig. S3.
Evolution of the percentage of sp^2 atoms with the carbon content for GO, rGO, MW-rGO, CVD-grown graphene and graphite obtained from the deconvolution of the C1s regions presented in Fig. 1B. After microwaving, reduced graphene oxide possesses high amount of carbon, similar to graphite and graphene, and a high percentage of sp^2 suggesting a large restoration of the conjugated network of the nanosheets in perfect agreement with Raman spectroscopy.

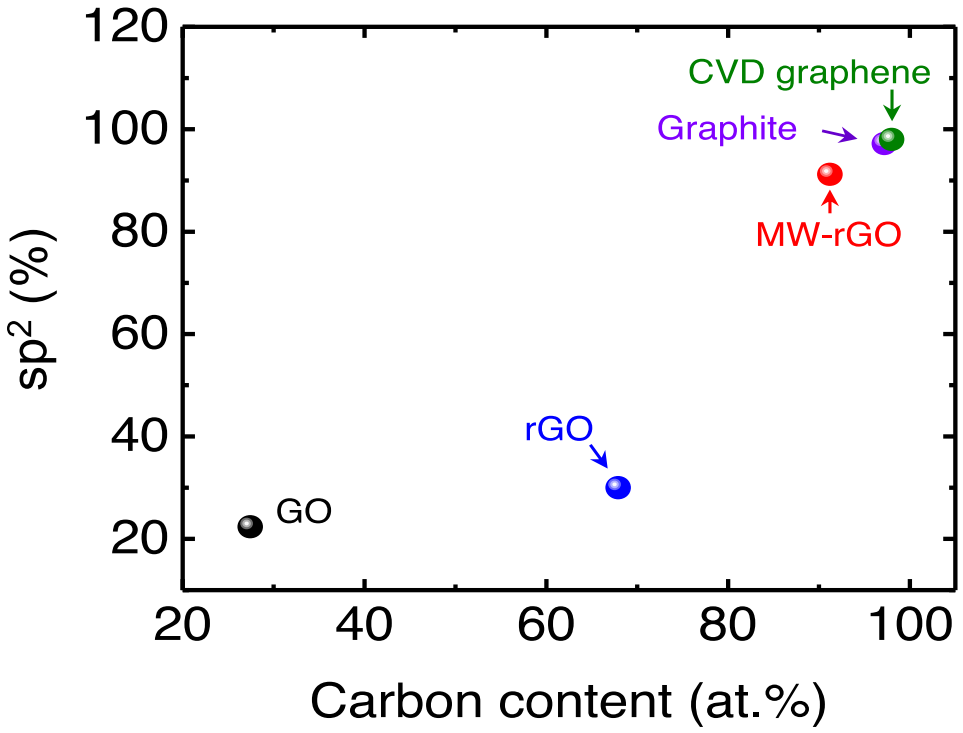

Calculation of the carrier mobility

The carrier mobility was calculated from the transfer characteristics of the transistors following methods from the literature (*55*, *56*). The carrier concentration has been estimated using Equation *(Eq. IV)*:

$$|V_G - V_{G\,min}| = \frac{h \times v_F \times \sqrt{\pi n}}{e} + \frac{ne}{C_{dl}} \text{ (Eq. IV)},$$

Where h, v_F, e and V_G represent the reduced Planck's constant, the Fermi velocity for the Dirac cone electrons, the electron charge and the gate potential respectively.

The mobility (μ) was then obtained from Equation *(Eq. V)*:

$$\mu = \left(\frac{d\sigma}{dn}\right) \times \frac{1}{e} \text{ (Eq. V)},$$

Where σ is the conductivity of the channel. Numerous FET devices were fabricated and tested using 6 different batches of graphene oxide (Fig. S4). High carrier mobilities are consistently obtained from MW-rGO samples confirming the high quality of the microwave reduction.

Fig. S4.
Carrier mobilities of MW-rGO measured at V_{ds} = 25 mV, 50 mV and 100 mV.

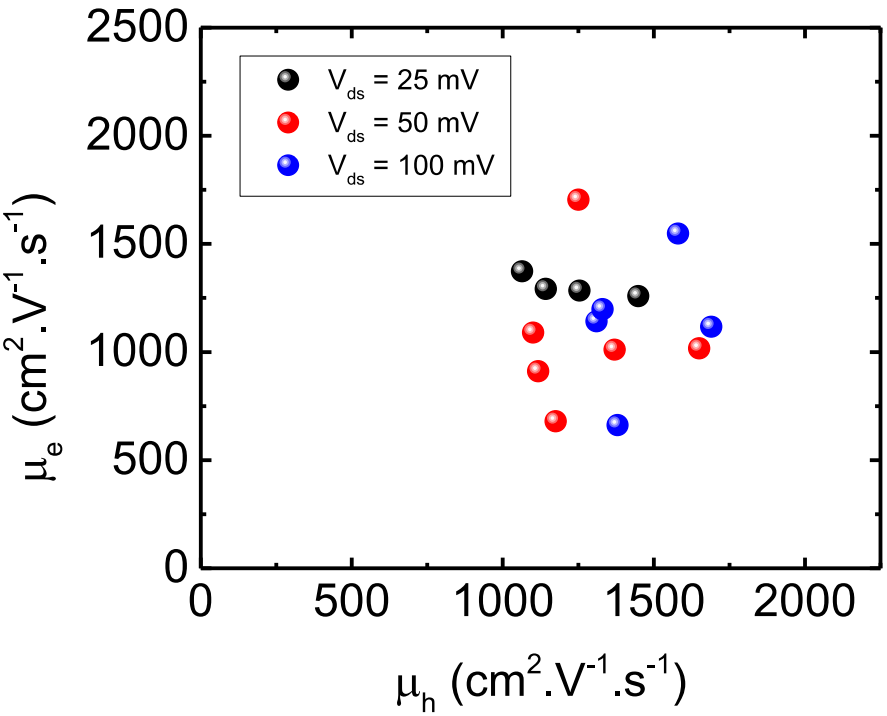

Electrodeposition of Ni-Fe layered double hydroxide (LDH) nanosheets

Ni-Fe LDH was electrodeposited on the MW-rGO (rGO) nanosheets using a 3-electrode cell as described above. A 5 mM aqueous solution of $Ni(NO_3)_2$ and $Fe(NO_3)_3$ with a molar ratio Ni:Fe=1:1 was used as electrolyte and as source of Ni and Fe (*57*). Electrodeposition of Ni-Fe LDH nanosheets was achieved by applying a constant potential of -1000 mV for 60 s-300 s. The deposition time have been optimized and we

found that 240 s gives the best performance in term of current density and overpotential. After deposition, the electrodes were rinsed with water and ethanol and finally dried in air.

The MW-rGO and rGO fibers were observed by scanning electron microscopy (Fig. S5). We observed similar physical structure of the NiFe LDH nanosheets on both supports suggesting that the intrinsic activity and the amount of active sites don't vary significantly between MW-rGO and the rGO.

Fig. S5.
Scanning electron microscopy images of NiFe@rGO (**A**) and NiFe@MW-rGO (**B**) showing that NiFe LDH has similar structure on both rGO and MW-rGO substrates.

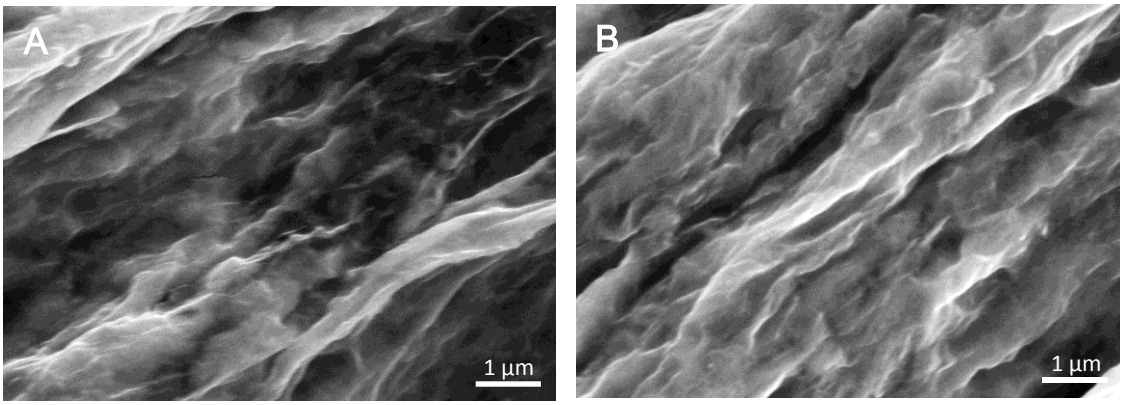

Preparation of the HER electrodes

The HER electrodes were prepared by depositing amorphous MoS_X on the reduced GO nanosheets. rGO and MW-rGO nanosheets were dip-coated in a saturated $(NH_4)_2MoS_4$ aqueous solution (Sigma-Aldrich). After deposition the electrodes were rinsed with water and ethanol and dried.

Hydrogen evolution reaction (HER)

HER ($2H^+ + 2e^- = H_2$) measurements were performed in a 0.5 M H_2SO_4 solution. Electrodes were cycled as described above. Cycling voltammetry was then performed between +100 mV and – 700 mV vs. the reference electrode at a scan rate of 5 $mV.s^{-1}$. The SCE electrode was calibrated against platinum under 1 bar of H_2 in a 0.5 M H_2SO_4 solution saturated with H_2. We measured in 0.5 M H_2SO_4:

$$E_{RHE} = E_{SCE} + 256\ mV$$

Figs. S6A,B show the polarization curves and the corresponding Tafel plots for the MoS_X@rGO and MoS_X@MW-rGO electrodes. In the case of MW-rGO, there is a dramatic increase of the absolute current density together with a decrease of the overpotential. Onset-potentials as low as ~ 100 mV are obtained when using MW-rGO as conducting support. Similar improvement of the electrocatalytic behavior is observed for the Tafel slope with a decrease of the Tafel slope from > 300 mV/dec for MoS_X@rGO down to ~ 50 mV mV/dec for MoS_X@MW-rGO (Figs. S6B). Such large decrease of the Tafel demonstrates the improved kinetics at the active sites due to faster electron transfer between MW-rGO and MoS_X. This is also supported by the EIS data (Fig. S6C) that

shows that both the internal resistance (Z_S) and the charge transfer resistance (Z_{CT}) are significantly reduced when using microwaved reduced graphene oxide. Notably the internal resistance drops from 1250 Ω to < 15 Ω thanks to the high conductivity of MW-rGO.

Finally the stability of the MoS_X@MW-rGO electrode was tested over 100 hours to ensure that the electrodes sustain high activity over long period of times. Fig. S6D shows the galvanostatic measurements for both MoS_X@rGO and MoS_X@MW-rGO during 100 hours. Results demonstrate the perfect stability of the MW-rGO electrode with a virtually constant overpotential to supply 10 $mA.cm^{-2}$.

Fig. S6.
(**A**) Polarization curves obtained for MoS_X@MW-rGO and MoS_X@rGO electrodes measured in 0.5 M H_2SO_4 showing the large improvement of the HER activity in the case of MoS_X@MW-rGO. (**B**) Corresponding Tafel plots. (**C**) Electrochemical impedance spectroscopy of MoS_X on rGO and MW-rGO. Internal resistance (Z_S) and charge transfer resistance (Z_{CT}) are significantly reduced to 15 Ω and 160 Ω respectively when using MW-rGO due to the combined effect of the high conductivity of microwaved graphene oxide and the low contact resistance from MW-rGO to MoS_X. (**D**) Galvanostatic measurements over 100 h at 10 $mA.cm^{-2}$ for MoS_X@rGO and MoS_X@MW-rGO showing the perfect stability of MW-rGO electrodes.

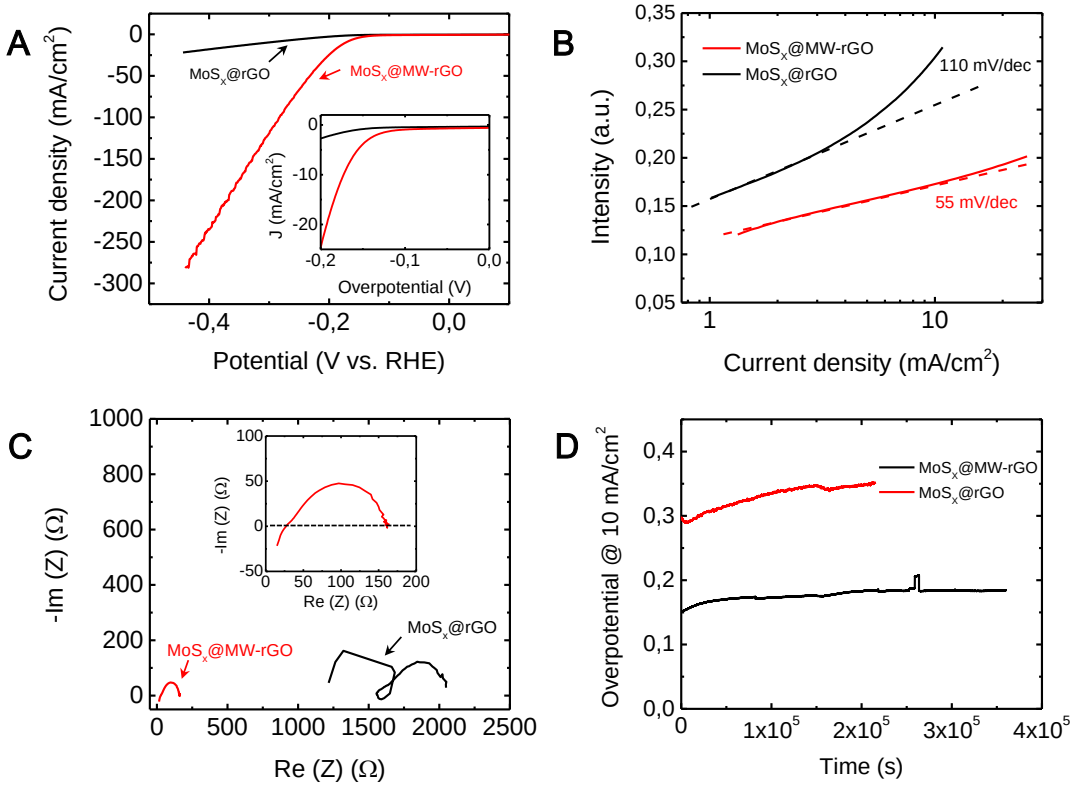

References and Notes

1. S. Park, R. S. Ruoff, Chemical methods for the production of graphenes. *Nat. Nanotechnol.* **4**, 217–224 (2009).doi:10.1038/nnano.2009.58 Medline

2. K. P. Loh, Q. Bao, P. K. Ang, J. Yang, The chemistry of graphene. *J. Mater. Chem.* **20**, 2277–2289 (2010). doi:10.1039/b920539j

3. K. R. Paton, E. Varrla, C. Backes, R. J. Smith, U. Khan, A. O'Neill, C. Boland, M. Lotya, O. M. Istrate, P. King, T. Higgins, S. Barwich, P. May, P. Puczkarski, I. Ahmed, M. Moebius, H. Pettersson, E. Long, J. Coelho, S. E. O'Brien, E. K. McGuire, B. M. Sanchez, G. S. Duesberg, N. McEvoy, T. J. Pennycook, C. Downing, A. Crossley, V. Nicolosi, J. N. Coleman, Scalable production of large quantities of defect-free few-layer graphene by shear exfoliation in liquids. *Nat. Mater.* **13**, 624–630 (2014).doi:10.1038/nmat3944 Medline

4. K. P. Loh, Q. Bao, G. Eda, M. Chhowalla, Graphene oxide as a chemically tunable platform for optical applications. *Nat. Chem.* **2**, 1015–1024 (2010).doi:10.1038/nchem.907 Medline

5. C.-Y. Su, Y. Xu, W. Zhang, J. Zhao, X. Tang, C.-H. Tsai, L.-J. Li, Electrical and spectroscopic characterizations of ultra-large reduced graphene oxide monolayers. *Chem. Mater.* **21**, 5674–5680 (2009). doi:10.1021/cm902182y

6. J. Zhao, S. Pei, W. Ren, L. Gao, H.-M. Cheng, Efficient preparation of large-area graphene oxide sheets for transparent conductive films. *ACS Nano* **4**, 5245–5252 (2010).doi:10.1021/nn1015506 Medline

7. Q. Zheng, W. H. Ip, X. Lin, N. Yousefi, K. K. Yeung, Z. Li, J.-K. Kim, Transparent conductive films consisting of ultralarge graphene sheets produced by Langmuir-Blodgett assembly. *ACS Nano* **5**, 6039–6051 (2011).doi:10.1021/nn2018683 Medline

8. I. Jung, D. A. Dikin, R. D. Piner, R. S. Ruoff, Tunable electrical conductivity of individual graphene oxide sheets reduced at "low" temperatures. *Nano Lett.* **8**, 4283–4287 (2008).doi:10.1021/nl8019938 Medline

9. K. Erickson, R. Erni, Z. Lee, N. Alem, W. Gannett, A. Zettl, Determination of the local chemical structure of graphene oxide and reduced graphene oxide. *Adv. Mater.* **22**, 4467–4472 (2010).doi:10.1002/adma.201000732 Medline

10. E. Yoo, T. Okata, T. Akita, M. Kohyama, J. Nakamura, I. Honma, Enhanced electrocatalytic activity of Pt subnanoclusters on graphene nanosheet surface. *Nano Lett.* **9**, 2255–2259 (2009).doi:10.1021/nl900397t Medline

11. Y. Liang, Y. Li, H. Wang, J. Zhou, J. Wang, T. Regier, H. Dai, Co_3O_4 nanocrystals on graphene as a synergistic catalyst for oxygen reduction reaction. *Nat. Mater.* **10**, 780–786 (2011).doi:10.1038/nmat3087 Medline

12. Y. Li, H. Wang, L. Xie, Y. Liang, G. Hong, H. Dai, MoS_2 nanoparticles grown on graphene: An advanced catalyst for the hydrogen evolution reaction. *J. Am. Chem. Soc.* **133**, 7296–7299 (2011).doi:10.1021/ja201269b Medline

13. J. Yang, D. Voiry, S. J. Ahn, D. Kang, A. Y. Kim, M. Chhowalla, H. S. Shin, Two-dimensional hybrid nanosheets of tungsten disulfide and reduced graphene oxide as catalysts for enhanced hydrogen evolution. *Angew. Chem. Int. Ed.* **52**, 13751–13754 (2013).doi:10.1002/anie.201307475 Medline

14. M. D. Stoller, S. Park, Y. Zhu, J. An, R. S. Ruoff, Graphene-based ultracapacitors. *Nano Lett.* **8**, 3498–3502 (2008).doi:10.1021/nl802558y Medline

15. J. G. Radich, P. V. Kamat, Origin of reduced graphene oxide enhancements in electrochemical energy storage. *ACS Catal.* **2**, 807–816 (2012). doi:10.1021/cs3001286

16. H. Wang, L.-F. Cui, Y. Yang, H. Sanchez Casalongue, J. T. Robinson, Y. Liang, Y. Cui, H. Dai, Mn_3O_4-graphene hybrid as a high-capacity anode material for lithium ion batteries. *J. Am. Chem. Soc.* **132**, 13978–13980 (2010).doi:10.1021/ja105296a Medline

17. H. Wang, Y. Yang, Y. Liang, J. T. Robinson, Y. Li, A. Jackson, Y. Cui, H. Dai, Graphene-wrapped sulfur particles as a rechargeable lithium-sulfur battery cathode material with high capacity and cycling stability. *Nano Lett.* **11**, 2644–2647 (2011).doi:10.1021/nl200658a Medline

18. G. Yu, L. Hu, M. Vosgueritchian, H. Wang, X. Xie, J. R. McDonough, X. Cui, Y. Cui, Z. Bao, Solution-processed graphene/MnO_2 nanostructured textiles for high-performance electrochemical capacitors. *Nano Lett.* **11**, 2905–2911 (2011).doi:10.1021/nl2013828 Medline

19. W. S. Hummers Jr., R. E. Offeman, Preparation of graphitic oxide. *J. Am. Chem. Soc.* **80**, 1339 (1958). doi:10.1021/ja01539a017

20. G. Eda, G. Fanchini, M. Chhowalla, Large-area ultrathin films of reduced graphene oxide as a transparent and flexible electronic material. *Nat. Nanotechnol.* **3**, 270–274 (2008).doi:10.1038/nnano.2008.83 Medline

21. D. A. Dikin, S. Stankovich, E. J. Zimney, R. D. Piner, G. H. B. Dommett, G. Evmenenko, S. T. Nguyen, R. S. Ruoff, Preparation and characterization of graphene oxide paper. *Nature* **448**, 457–460 (2007).doi:10.1038/nature06016 Medline

22. R. Cruz-Silva, A. Morelos-Gomez, H. I. Kim, H. K. Jang, F. Tristan, S. Vega-Diaz, L. P. Rajukumar, A. L. Elías, N. Perea-Lopez, J. Suhr, M. Endo, M. Terrones, Super-stretchable graphene oxide macroscopic fibers with outstanding knotability fabricated by dry film scrolling. *ACS Nano* **8**, 5959–5967 (2014).doi:10.1021/nn501098d Medline

23. G. Xin, T. Yao, H. Sun, S. M. Scott, D. Shao, G. Wang, J. Lian, Highly thermally conductive and mechanically strong graphene fibers. *Science* **349**, 1083–1087 (2015).doi:10.1126/science.aaa6502 Medline

24. S. Park, Y. Hu, J. O. Hwang, E.-S. Lee, L. B. Casabianca, W. Cai, J. R. Potts, H.-W. Ha, S. Chen, J. Oh, S. O. Kim, Y.-H. Kim, Y. Ishii, R. S. Ruoff, Chemical structures of hydrazine-treated graphene oxide and generation of aromatic nitrogen doping. *Nat. Commun.* **3**, 638 (2012).doi:10.1038/ncomms1643 Medline

25. I. K. Moon, J. Lee, R. S. Ruoff, H. Lee, Reduced graphene oxide by chemical graphitization. *Nat. Commun.* **1**, 73 (2010).doi:10.1038/ncomms1067 Medline

26. X. Li, G. Zhang, X. Bai, X. Sun, X. Wang, E. Wang, H. Dai, Highly conducting graphene sheets and Langmuir-Blodgett films. *Nat. Nanotechnol.* **3**, 538–542 (2008).doi:10.1038/nnano.2008.210 Medline

27. G. Eda, Y.-Y. Lin, C. Mattevi, H. Yamaguchi, H.-A. Chen, I.-S. Chen, C.-W. Chen, M. Chhowalla, Blue photoluminescence from chemically derived graphene oxide. *Adv. Mater.* **22**, 505–509 (2010).doi:10.1002/adma.200901996 Medline

28. Z. Luo, P. M. Vora, E. J. Mele, A. T. C. Johnson, J. M. Kikkawa, Photoluminescence and band gap modulation in graphene oxide. *Appl. Phys. Lett.* **94**, 111909 (2009). doi:10.1063/1.3098358

29. D. R. Dreyer, S. Park, C. W. Bielawski, R. S. Ruoff, The chemistry of graphene oxide. *Chem. Soc. Rev.* **39**, 228–240 (2010).doi:10.1039/B917103G Medline

30. R. Larciprete, S. Fabris, T. Sun, P. Lacovig, A. Baraldi, S. Lizzit, Dual path mechanism in the thermal reduction of graphene oxide. *J. Am. Chem. Soc.* **133**, 17315–17321 (2011).doi:10.1021/ja205168x Medline

31. J. Kotakoski, A. V. Krasheninnikov, K. Nordlund, Energetics, structure, and long-range interaction of vacancy-type defects in carbon nanotubes: Atomistic simulations. *Phys. Rev. B* **74**, 245420 (2006). doi:10.1103/PhysRevB.74.245420

32. A. Bagri, C. Mattevi, M. Acik, Y. J. Chabal, M. Chhowalla, V. B. Shenoy, Structural evolution during the reduction of chemically derived graphene oxide. *Nat. Chem.* **2**, 581–587 (2010).doi:10.1038/nchem.686 Medline

33. Z. Luo, Y. Lu, L. A. Somers, A. T. C. Johnson, High yield preparation of macroscopic graphene oxide membranes. *J. Am. Chem. Soc.* **131**, 898–899 (2009).doi:10.1021/ja807934n Medline

34. H. A. Becerril, J. Mao, Z. Liu, R. M. Stoltenberg, Z. Bao, Y. Chen, Evaluation of solution-processed reduced graphene oxide films as transparent conductors. *ACS Nano* **2**, 463–470 (2008).doi:10.1021/nn700375n Medline

35. S. Wang, P. K. Ang, Z. Wang, A. L. L. Tang, J. T. L. Thong, K. P. Loh, High mobility, printable, and solution-processed graphene electronics. *Nano Lett.* **10**, 92–98 (2010).doi:10.1021/nl9028736 Medline

36. See supplementary materials.

37. Y. Zhu, S. Murali, M. D. Stoller, A. Velamakanni, R. D. Piner, R. S. Ruoff, Microwave assisted exfoliation and reduction of graphite oxide for ultracapacitors. *Carbon* **48**, 2118–2122 (2010). doi:10.1016/j.carbon.2010.02.001

38. W. Chen, L. Yan, P. R. Bangal, Preparation of graphene by the rapid and mild thermal reduction of graphene oxide induced by microwaves. *Carbon* **48**, 1146–1152 (2010). doi:10.1016/j.carbon.2009.11.037

39. H. Hu, Z. Zhao, Q. Zhou, Y. Gogotsi, J. Qiu, The role of microwave absorption on formation of graphene from graphite oxide. *Carbon* **50**, 3267–3273 (2012). doi:10.1016/j.carbon.2011.12.005

40. H. Feng, R. Cheng, X. Zhao, X. Duan, J. Li, A low-temperature method to produce highly reduced graphene oxide. *Nat. Commun.* **4**, 1539 (2013).doi:10.1038/ncomms2555 Medline

41. K. Parvez, Z.-S. Wu, R. Li, X. Liu, R. Graf, X. Feng, K. Müllen, Exfoliation of graphite into graphene in aqueous solutions of inorganic salts. *J. Am. Chem. Soc.* **136**, 6083–6091 (2014).doi:10.1021/ja5017156 Medline

42. S. Eigler, M. Enzelberger-Heim, S. Grimm, P. Hofmann, W. Kroener, A. Geworski, C. Dotzer, M. Röckert, J. Xiao, C. Papp, O. Lytken, H.-P. Steinrück, P. Müller, A. Hirsch, Wet chemical synthesis of graphene. *Adv. Mater.* **25**, 3583–3587 (2013).doi:10.1002/adma.201300155 Medline

43. N. Petrone, C. R. Dean, I. Meric, A. M. van der Zande, P. Y. Huang, L. Wang, D. Muller, K. L. Shepard, J. Hone, Chemical vapor deposition-derived graphene with electrical performance of exfoliated graphene. *Nano Lett.* **12**, 2751–2756 (2012).doi:10.1021/nl204481s Medline

44. I. McCulloch, A. Salleo, M. Chabinyc, Avoid the kinks when measuring mobility. *Science* **352**, 1521–1522 (2016).doi:10.1126/science.aaf9062 Medline

45. T. Shinagawa, A. T. Garcia-Esparza, K. Takanabe, Insight on Tafel slopes from a microkinetic analysis of aqueous electrocatalysis for energy conversion. *Sci. Rep.* **5**, 13801 (2015).doi:10.1038/srep13801 Medline

46. X. Li, C. W. Magnuson, A. Venugopal, J. An, J. W. Suk, B. Han, M. Borysiak, W. Cai, A. Velamakanni, Y. Zhu, L. Fu, E. M. Vogel, E. Voelkl, L. Colombo, R. S. Ruoff, Graphene films with large domain size by a two-step chemical vapor deposition process. *Nano Lett.* **10**, 4328–4334 (2010).doi:10.1021/nl101629g Medline

47. M. S. Dresselhaus, A. Jorio, M. Hofmann, G. Dresselhaus, R. Saito, Perspectives on carbon nanotubes and graphene Raman spectroscopy. *Nano Lett.* **10**, 751–758 (2010).doi:10.1021/nl904286r Medline

48. A. C. Ferrari, J. C. Meyer, V. Scardaci, C. Casiraghi, M. Lazzeri, F. Mauri, S. Piscanec, D. Jiang, K. S. Novoselov, S. Roth, A. K. Geim, Raman spectrum of graphene and graphene layers. *Phys. Rev. Lett.* **97**, 187401 (2006).doi:10.1103/PhysRevLett.97.187401 Medline

49. A. C. Ferrari, D. M. Basko, Raman spectroscopy as a versatile tool for studying the properties of graphene. *Nat. Nanotechnol.* **8**, 235–246 (2013).doi:10.1038/nnano.2013.46 Medline

50. L. G. Cançado, A. Jorio, E. H. M. Ferreira, F. Stavale, C. A. Achete, R. B. Capaz, M. V. O. Moutinho, A. Lombardo, T. S. Kulmala, A. C. Ferrari, Quantifying defects in graphene via Raman spectroscopy at different excitation energies. *Nano Lett.* **11**, 3190–3196 (2011).doi:10.1021/nl201432g Medline

51. L. G. Cançado, K. Takai, T. Enoki, M. Endo, Y. A. Kim, H. Mizusaki, A. Jorio, L. N. Coelho, R. Magalhães-Paniago, M. A. Pimenta, General equation for the determination of the crystallite size L_a of nanographite by Raman spectroscopy. *Appl. Phys. Lett.* **88**, 163106 (2006). doi:10.1063/1.2196057

52. S. Stankovich, D. A. Dikin, R. D. Piner, K. A. Kohlhaas, A. Kleinhammes, Y. Jia, Y. Wu, S. B. T. Nguyen, R. S. Ruoff, Synthesis of graphene-based nanosheets via chemical reduction of exfoliated graphite oxide. *Carbon* **45**, 1558–1565 (2007). doi:10.1016/j.carbon.2007.02.034

53. J. Zhang, H. Yang, G. Shen, P. Cheng, J. Zhang, S. Guo, Reduction of graphene oxide via L-ascorbic acid. *Chem. Commun.* **46**, 1112–1114 (2010).doi:10.1039/B917705A Medline

54. C. Mattevi, G. Eda, S. Agnoli, S. Miller, K. A. Mkhoyan, O. Celik, D. Mastrogiovanni, G. Granozzi, E. Garfunkel, M. Chhowalla, Evolution of electrical, chemical, and structural properties of transparent and conducting chemically derived graphene thin films. *Adv. Funct. Mater.* **19**, 2577–2583 (2009). doi:10.1002/adfm.200900166

55. F. Chen, Q. Qing, J. Xia, J. Li, N. Tao, Electrochemical gate-controlled charge transport in graphene in ionic liquid and aqueous solution. *J. Am. Chem. Soc.* **131**, 9908–9909 (2009).doi:10.1021/ja9041862 Medline

56. S.-K. Lee, B. J. Kim, H. Jang, S. C. Yoon, C. Lee, B. H. Hong, J. A. Rogers, J. H. Cho, J.-H. Ahn, Stretchable graphene transistors with printed dielectrics and gate electrodes. *Nano Lett.* **11**, 4642–4646 (2011).doi:10.1021/nl202134z Medline

57. X. Lu, C. Zhao, Electrodeposition of hierarchically structured three-dimensional nickel-iron electrodes for efficient oxygen evolution at high current densities. *Nat. Commun.* **6**, 6616 (2015).doi:10.1038/ncomms7616 Medline